

The Low-Lying Dirac Spectrum of Staggered Quarks

E. Follana,¹ A. Hart,² C.T.H. Davies,¹ and Q. Mason³
(HPQCD and UKQCD collaborations)

¹*Department of Physics and Astronomy, University of Glasgow, Glasgow G12 8QQ, U.K.*

²*School of Physics, University of Edinburgh, King's Buildings, Edinburgh EH9 3JZ, U.K.*

³*Department of Applied Mathematics and Theoretical Physics, University of Cambridge, Cambridge, U.K.*

We investigate and clarify the role of topology and the issues surrounding the ε -regime for staggered quarks. We study unimproved and improved staggered quark Dirac operators on quenched lattice QCD gluon backgrounds generated using a Symanzik-improved gluon action. For the improved Dirac operators we find a clear separation of the spectrum into would-be zero modes and others. The number of would-be zero modes depends on the topological charge as predicted by the continuum Index Theorem, and the expectation values of their chirality are large for the most improved actions (≈ 0.7). The remaining modes have low chirality and show clear signs of clustering into quartets that become degenerate in the continuum limit. We demonstrate that the lattice spacing and volume dependence of the eigenvalues follow expectations. Furthermore, the non-zero modes follow the random matrix theory predictions for all topological charge sectors. The values of the chiral condensate extracted from fits to the theoretical distributions are consistent with each other, and with the results obtained from the total density of eigenvalues using the Banks-Casher relation. We conclude that staggered quarks respond correctly to QCD topology when both fermion and gauge actions are improved.

PACS numbers: 11.15.Ha, 12.38.Gc

I. INTRODUCTION

The low energy regime of Quantum Chromodynamics (QCD) exhibits a rich and interesting phenomenology, including the $U_A(1)$ axial anomaly, chiral symmetry breaking and the topological properties of the theory. A crucial step in elucidating these effects is understanding the low-lying eigenvalue spectrum of the Dirac operator. There are a number of detailed predictions of the properties of these low-lying modes, such as the existence of an Index Theorem, the Banks-Casher relation, and the distribution of the first few eigenvalues in fixed topological charge sectors. Such effects are, however, inherently non-perturbative and can only be studied fully using techniques like lattice Monte Carlo simulation.

Universality decrees that any correct discretization of QCD must be correct close enough to the continuum limit. If we want to make phenomenological predictions, however, it is crucial that the QCD lattice Dirac operator also has the correct low-lying spectrum at the lattice spacings typically simulated. By this we mean that the deformations to the eigenvalue spectrum brought about by the discretization must be small. In this case the relevant scale for comparison is the light sea quark mass, $m_{u,d} = \mathcal{O}(5 \text{ MeV})$.

In this paper we show that these deformations are small enough for one particular class of lattice fermions that are widely used in large scale lattice simulations: improved staggered quarks. Working at similar lattice spacings in the quenched theory (i.e. pure Yang-Mills gluodynamics) we show that the low-lying QCD Dirac eigenvalue spectrum very closely reproduces the continuum features. In particular, we show that improved staggered fermions do respond correctly to the gluonic topo-

logical charge, and discuss why some confusion on this issue exists in the literature.

To reach these conclusions we test a number of predictions, quantitative and qualitative, for the low-lying modes: the Atiyah-Singer Index Theorem, that relates the zero modes to the topological charge of the gauge field; the Banks-Casher relation, linking the chiral condensate to the density of eigenvalues at the origin; the universality of the low-lying eigenvalue spectrum in the ε -regime, and its connection to Random Matrix Theory. In addition, we change both the lattice spacing and volume and show that the variation of the spectrum matches theoretical expectations.

This paper expands and refines the work in [1, 2]. We include much more extensive data, both on larger volumes and finer lattices. Related work has been presented in [3, 4].

The structure of the paper is as follows. In Sec. II we describe our expectations for the Dirac eigenvalue spectrum, both in the continuum and with lattice staggered fermions. We also review the existing literature. We describe our methodology in Sec. III, and discuss the features of the spectrum in Sec. IV. In Sec. V we compare our results for the low-lying eigenvalues with the universal predictions from random matrix theory. We summarise and conclude our study in Sec. VI.

II. THEORETICAL BACKGROUND

In this section we review the theoretical expectations for the spectrum of the Dirac operator in the continuum and lattice staggered cases.

A. Continuum QCD

A single, continuum fermion species is described by the massless, gauge covariant Dirac operator, which is anti-Hermitian with a purely imaginary eigenvalue spectrum:

$$\mathcal{D}f_s = i\lambda_s f_s, \quad \lambda_s \in \mathbb{R}. \quad (1)$$

Choosing orthonormalised eigenvectors, satisfying

$$f_s^\dagger f_t = \delta_{st}, \quad (2)$$

the chirality of an eigenvector is defined by

$$\chi_s \equiv f_s^\dagger \gamma_5 f_s. \quad (3)$$

The Dirac operator also anticommutes with γ_5 ,

$$\{\mathcal{D}, \gamma_5\} = 0, \quad (4)$$

implying that the spectrum is symmetric about zero:

$$\text{sp}(\mathcal{D}) = \{\pm i\lambda_s, \lambda_s \in \mathbb{R}\}. \quad (5)$$

If $\lambda_s \neq 0$, then $\gamma_5 f_s$ is also an eigenvector with eigenvalue $-i\lambda_s$, and zero chirality, $\chi_s = 0$. The zero modes, $\lambda_s = 0$, can be chosen with definite chirality, $\chi_s = \pm 1$.

1. Topological charge and the Index Theorem

Smooth continuum gauge field configurations can be classified by their winding number, which is an integer given by the expression:

$$Q = \frac{1}{32\pi^2} \int d^4x \epsilon_{\mu\nu\sigma\tau} \text{Tr} F_{\mu\nu}(x) F_{\sigma\tau}(x). \quad (6)$$

If we now consider the Dirac operator in the given gauge background, and we denote by n_\pm the number of zero modes with a given chirality, their difference is related to the topological charge via the Atiyah–Singer Index Theorem [5, 6]:

$$Q = m \text{Tr} \frac{\gamma_5}{\mathcal{D}(A) + m} = \sum_s \chi_s = n_+ - n_-, \quad (7)$$

where m is the quark mass (we keep the sign conventions of Ref. [1]).

2. The chiral condensate and the Banks–Casher relation

The bare chiral condensate in a given gauge field background, A , is given by the trace over the quark propagator:

$$\langle \bar{\psi}\psi(m) \rangle = -\frac{1}{V} \text{Tr} \frac{1}{\mathcal{D}(A) + m}. \quad (8)$$

In the limit of $m \rightarrow 0$ it acts as an order parameter for the spontaneous breaking of chiral symmetry. Expanding in eigenmodes of \mathcal{D} and using the $\pm i\lambda_s$ symmetry,

$$\langle \bar{\psi}\psi(m) \rangle = -\frac{1}{V} \sum_s \frac{1}{i\lambda_s + m} = -\frac{m}{V} \sum_s \frac{1}{\lambda_s^2 + m^2}. \quad (9)$$

Averaging over a full ensemble of gauge fields, the sum over s can be replaced by an integral over eigenvalues with measure given by the spectral density:

$$\rho(\lambda) \equiv \frac{1}{V} \sum_s \delta(\lambda - \lambda_s). \quad (10)$$

The integral has a smooth limit as $m \rightarrow 0$:

$$\begin{aligned} \Sigma \equiv -\langle \bar{\psi}\psi(m=0) \rangle &= \lim_{m \rightarrow 0} m \int_{-\infty}^{\infty} d\lambda \frac{\rho(\lambda)}{\lambda^2 + m^2} \\ &= \pi\rho(0), \end{aligned} \quad (11)$$

which is the Banks–Casher relation. We expect the chiral condensate Σ to be non-zero when the chiral symmetry is spontaneously broken. This requires that the large volume limit is taken before $m \rightarrow 0$ to ensure that the discrete sum over eigenmodes can be replaced by the smooth integral.

3. The ε -regime and spectral universality

The ε -regime of QCD occurs when the theory is regularised in a finite volume such that the typical system size L satisfies

$$\varepsilon\text{-regime:} \quad (\Lambda_{\text{QCD}})^{-1} \ll L \ll (M_\pi)^{-1}. \quad (12)$$

In such systems, the volume is large enough that we may derive an effective chiral field theory for pions by integrating out all other hadronic states. The typical Compton wavelength of the particles so removed is $(\Lambda_{\text{QCD}})^{-1}$. At the same time, the system is very small compared to the Compton wavelength of the pions, so we can further integrate out all their kinetic modes to leave us with a theory describing just static pions.

It can then be rigorously shown that the remaining finite volume partition function exactly corresponds to that of a random matrix theory (RMT) with the same chiral symmetries as QCD [7, 8]. This universality [9, 10] allows us to predict the distributions of low-lying non-zero eigenvalues of the Dirac operator using RMT [11, 12]. The relevant universality class is determined by the chiral symmetries of the finite volume partition function, and hence of QCD; for fermions in the fundamental representation of the gauge group with $N_c \geq 3$ the appropriate class is the chiral Unitary Ensemble (chUE) with Dyson index $\beta = 2$.

Rather than the absolute eigenvalue spacings, RMT predicts only the *relative* spacings of the eigenvalues in the form of *microscopic* (or *unfolded*) spectral densities

$\rho_s(z)$. These detail the universal distribution of one or more eigenvalues. There are separate predictions for each sector of topological charge. The absolute spectral densities include a QCD-specific scale factor based on the chiral condensate:

$$\rho(\lambda) = \Sigma V \rho_s(\lambda \Sigma V). \quad (13)$$

Comparison of the Dirac spectrum with RMT therefore provides a method of determining the chiral symmetries of QCD, of probing the role of topology, and of measuring the chiral condensate.

For the combined spectral density of all eigenvalues in a given topological charge sector RMT predicts [13]

$$\rho_{\text{all}}(z) = \frac{z}{2} [J_\nu^2(z) - J_{\nu+1}(z)J_{\nu-1}(z)], \quad (14)$$

where $J_\nu(z)$ are Bessel functions and $\nu = |Q|$. As these and all other predictions depend only on $|Q|$, we improve the statistical accuracy of the comparison with the Dirac spectrum by combining the $\pm|Q|$ sub-ensembles.

There are also separate predictions for the k^{th} eigenvalue [12, 14], e.g. $k = 1$:

$$\rho_1(z) = \begin{cases} \frac{z}{2} e^{-z^2/4}, & (\nu = 0), \\ \frac{z}{2} I_2(z) e^{-z^2/4}, & (\nu = 1), \\ \frac{z}{2} (I_2^2(z) - I_3(z)I_1(z)) e^{-z^2/4}, & (\nu = 2). \end{cases} \quad (15)$$

Expressions for higher k are given in Ref. [12].

B. Lattice staggered fermions

The massless, gauge-invariant, ONE-LINK staggered Dirac operator on a $d = 4$ dimensional Euclidean lattice with spacing a is

$$\mathcal{D}(x, y) = \frac{1}{2au_0} \sum_{\mu=1}^d \eta_\mu(x) [U_\mu(x) \delta_{x+\hat{\mu}, y} - H.c.] \quad (16)$$

$$\eta_\nu(x) = (-1)^{\sum_{\mu < \nu} x_\mu} \quad (17)$$

with u_0 an optional tadpole-improvement factor given, in our case, by the fourth root of the mean plaquette. \mathcal{D} is antihermitian and obeys a remnant of the continuum γ_5 anticommutation relation:

$$\{\mathcal{D}, \epsilon\} = 0, \quad \text{with} \quad \epsilon(x) = (-1)^{\sum_{\mu=1}^d x_\mu}. \quad (18)$$

As in the continuum case, its spectrum is therefore purely imaginary, with eigenvalues occurring in complex conjugate pairs:

$$\text{sp}(\mathcal{D}) = \{\pm i\lambda_s, \lambda_s \in \mathbb{R}\}. \quad (19)$$

In fact, if f_s is an eigenvector with eigenvalue $i\lambda_s$, then ϵf_s is also an eigenvector with eigenvalue $-i\lambda_s$.

The corresponding action describes $N_t = 2^{d/2} = 4$ ‘‘tastes’’ of fermions which interact via unphysical ‘‘taste

breaking’’ interactions that vanish in the continuum limit as a^2 . In the limit $a \rightarrow 0$ there is an $SU(N_t) \otimes SU(N_t)$ chiral symmetry, and the spectrum is therefore an exact N_t -fold copy of that described in Sec. II A.

At finite lattice spacing the chiral symmetry group is reduced to $U(1) \otimes U(1)$ and we do not expect to see this picture, for example there will not be an exact Index Theorem anymore. The relevant operator for the Index Theorem must be a taste-singlet, γ_5^{ts} , to couple to the vacuum correctly [15]. It is a point split operator in all d -dimensions, which can be made gauge invariant by the insertion of the appropriate U fields. It does not anticommute with the staggered Dirac operator, $\{\mathcal{D}, \gamma_5^{ts}\} \neq 0$. This also implies that the chirality of the eigenmodes will not be exactly ± 1 or 0.

Exact zero eigenvalues only occur accidentally (and are completely excluded at non-zero fermion mass), and all the eigenmodes will in principle contribute in Eq. (7) [16]. Due to the simple properties

$$[\gamma_5^{ts}, \epsilon] = 0, \quad (20)$$

$$\epsilon^\dagger \epsilon = I, \quad (21)$$

each pair of eigenvectors $\{f_s, \epsilon f_s\}$ has the same chirality χ_s :

$$\langle \epsilon f_s | \gamma_5^{ts} | \epsilon f_s \rangle = \langle f_s | \epsilon^\dagger \gamma_5^{ts} \epsilon | f_s \rangle = \langle f_s | \gamma_5^{ts} | f_s \rangle. \quad (22)$$

All of the preceding considerations depend only on simple symmetry properties, and apply equally well to the improved staggered operators we have used in our work.

Early studies of the ONE-LINK staggered operator and unimproved, Wilson gauge action for coarse, thermalized lattices were done in [16, 17, 18, 19, 20]. There was no clear separation in the low-lying modes, either in eigenvalue or chirality. The low-lying ONE-LINK eigenvalues also did not follow the universal predictions for continuum QCD. In particular they showed no dependence on the topological charge sector [21, 22, 23, 24, 25].

In this study, however, we are interested in whether improvement of the gauge action and Dirac operator allow the continuum-like spectrum to be seen.

Certainly, some continuum features emerge using very smooth gauge backgrounds (obtained by either repeated cooling or discretising classical instanton solutions) [16, 17]. By contrast, here we are interested in thermalized, unsmoothed configurations at lattice spacings (and gauge actions) typical of lattice simulations, i.e. $a \approx 0.1$ fm. We conjecture that these failures of continuum predictions follow from the use of coarse lattices and unimproved actions, resulting in large taste changing interactions that ruin the continuum chiral symmetries. We shall show that the improved staggered operators introduced below allow all the continuum features of the spectrum to emerge.

That improvement allows this to happen at such lattice spacings is not entirely unexpected. QCD predicts that the topological susceptibility is suppressed as we reduce the sea quark mass. This is seen in simulations using

improved gauge and staggered fermion actions [26, 27, 28, 29]. With ONE-LINK staggered sea quarks no such variation is seen [26, 30, 31, 32, 33]. Other evidence for the beneficial effect of improved staggered operators was seen in the Schwinger model [34, 35, 36, 37, 38], as well as in QCD [1, 2, 35, 37].

1. Improved staggered fermions

The continuum chiral symmetry is broken by the (unphysical) taste-changing interactions. At leading order these involve exchange of an ultraviolet gluon of momentum $q \approx \pi/a$. Such interactions are perturbative for typical values of the lattice spacing. They can therefore be removed systematically using the method of Symanzik. This gives lattice operators with better taste symmetry and smaller scaling violations. We do this by smearing the gauge field to apply a form factor to the quark-gluon vertex and suppress the coupling between quarks and high-momentum gluons [39, 40, 41]. This amounts to replacing the gauge link U in Eq. (17) by a “fat” link: a weighted sum of staples as shown graphically in Fig. 1. The choice of weight factors, c_i , determines the degree of improvement. In this paper we compare three different, improved operators known as ASQTAD, FAT7XASQ and HYP.

The first two are based on the FAT7 operator which includes staples of length up to $7a$. We can remove all $\mathcal{O}(a^2)$ discretization errors (at tree level) by adding two more terms to the FAT7 prescription, including a Naik three-link term [42] and a five-link Lepage staple [39]. This operator is called ASQ, whereas ASQTAD is the tadpole improved version which aims to also reduce the radiative corrections to the scaling.

The improvement procedure may be iterated; for our most highly improved operator the original links are first FAT7 smeared and projected back onto the $SU(3)$ gauge group. These fattened links are then used to construct the ASQ operator. We call this operator FAT7XASQ. We stress that this is the same operator that was used in [1]. Regrettably, there it was misnamed HISQ, a name already used to describe a slightly different Dirac operator.

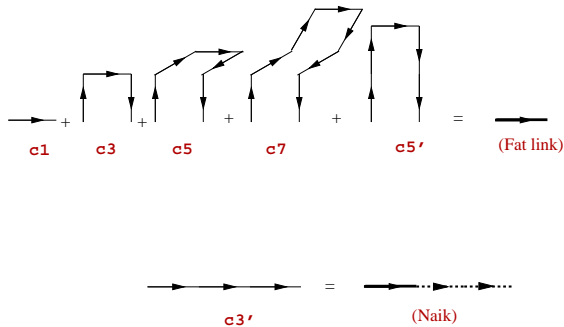


FIG. 1: Paths entering the improved staggered operators.

The final improved staggered Dirac operator is HYP [43]. Its construction is motivated by perfect action ideas, and involves three levels of (restricted) APE smearing with projection onto $SU(3)$ at each level. The restrictions are such that each fat link includes contributions only from thin links belonging to hypercubes attached to the original link.

The spectrum of all improved Dirac operators is of the form in Eq. (19). Improved operators, however, show very small taste-changing effects both in the hadronic splittings [20, 44] and, as we shall see, the eigenvalue spectrum.

III. DETAILS OF THE SIMULATION

In this section we provide details of the gauge backgrounds used in this study, and the methods used to determine the eigenvalues and the topological charge. We also introduce notation for the eigenvalues to be used in the following sections.

A. The gauge action

We use a quenched, $SU(3)$ gluonic action that is both tree level Symanzik and tadpole improved [45, 46, 47, 48, 49]:

$$S = -\beta \sum_x \sum_{\mu < \nu} \left(\frac{5}{3} P_{\mu\nu}(x) - \frac{1}{12} \frac{R_{\mu\mu\nu}(x)}{u_0^2} - \frac{1}{12} \frac{R_{\mu\nu\nu}(x)}{u_0^2} \right), \quad (23)$$

where P, R are 1×1 and 2×1 Wilson loops respectively. The tadpole improvement coefficient u_0 is defined as the fourth root of the mean plaquette.

We have generated five ensembles of around 1000 configurations, with parameters for these ensembles as in Table I (taken from Refs. [50, 51]). The physical spatial size of the lattice is aL , and the volume $a^4V \equiv a^4L^3T$. We have also used a few configurations from a Wilson gauge ensemble with lattice spacing $a \approx 0.1$ fm and volume $16^3 \times 32$.

Three ensembles have been tuned to study the effect of varying the lattice spacing at fixed physical volume ($aL \approx 1.5$ fm). Another three vary the volume at fixed $a = 0.093$ fm.

The two coarser lattice spacings are representative of current, large scale unquenched simulations using improved staggered quarks, with the smallest a being indicative of future calculations. Our gauge action differs from the one used by the MILC Collaboration [52] only in small one loop radiative corrections which do not affect the relevance of the results in this paper.

The main objective of this paper is to compare our results with the expectations from the continuum limit and with the predictions from RMT. For this purpose any systematic uncertainty in the determination of the lattice

TABLE I: Simulation parameters: the gauge coupling β , lattice spacing and volume and the spatial lattice extent.

β	a/fm	$V \equiv L^3T$	aL/fm
4.6	0.125	12^4	1.50
4.8	0.093	12^4	1.12
4.8	0.093	16^4	1.49
4.8	0.093	20^4	1.86
5.0	0.077	20^4	1.54

spacings (for example due to finite-volume effects) is not important. It would only become important for obtaining a precise determination of some physical quantity. Therefore in general we ignore this source of errors in our measurements, using only the statistical errors based on a jack-knife analysis of the data.

B. Measuring the topological charge

We measure the topological charge Q using a number of gluonic methods to look for consistency. The topological charge of a gluonic configuration is not uniquely defined at finite lattice spacing, and different methods will sometimes disagree. Over an ensemble, the number of configurations that disagree on the value of Q vanishes as a^2 in the continuum limit.

We first cool the gauge fields and then apply a lattice topological charge operator. The cooling is (separately) done with two different gauge actions (the Wilson and the 5Li [53, 54]). We measure the topological charge with the highly accurate “5 Loop improved” (5Li) operator [53, 54]. We then check that both charges are very close to integers and stable under cooling. If the topological charges (rounded to the nearest integer) defined by this procedure are the same for both actions, then we assign the configuration to a definite topological charge sector.

Does this consistency criterion bias our fixed- Q subensemble averages? No; at $a = 0.093$ fm ensembles fewer than 10% of the configurations have an ambiguous topological charge. For the finest ensemble, $a = 0.077$ fm, this number goes down to around 2%.

We have repeated parts of the analysis by ignoring the consistency requirement and using only one of the cooling actions in the definition of Q , assigning every configuration to a topological charge sector. The results are indistinguishable from those presented here, and therefore this robustness criterion neither introduces a systematic uncertainty in our results, nor changes the conclusions.

We stress that we only use cooling to determine the topological charge. All the Dirac spectrum measurements are done on the original thermalized (“hot”) configurations.

C. Determining the eigenvalues

To calculate the low-lying spectrum of the Dirac operators we use an implementation of the Cullum-Willoughby Lanczos-based algorithm [55]. Due to the structure of the staggered Dirac operator the calculation of the spectrum can be done on an hermitian, positive semi-definite operator, defined only on half of the lattice (either the odd or the even sublattice). The algorithm can be extended to the calculation of the corresponding eigenvectors, which are needed to obtain the chirality.

On the ensembles used in this study we found no significant numerical difficulties with this algorithm. In practice, the absence of exact zero modes simplifies the calculation from a numerical point of view, as the linear operator we are dealing with is then positive definite.

Due to the exact \pm symmetry, we only need to consider half of the spectrum, say $\{i\lambda_s, \lambda_s > 0\}$ (which we call the positive sector). The other half is a mirror image which we call the negative sector. From now on we dispense with the imaginary unit i , and discuss and show on the plots the imaginary part of the positive half spectrum $\{\lambda_s, \lambda_s > 0\}$.

For the analysis we divide the (positive) eigenmodes on each configuration into two sets based on the gluonic topological charge. Inspired by our continuum limit expectations, we expect the $4|Q|$ near-zero modes to divide into $2|Q|$ modes each side of zero. We call the arithmetic mean of the positive near-zero modes Λ_0 .

The remaining positive modes are divided into quartets. We call the means of successive sets $\Lambda_{1,2,\dots}$. We define the intra-quartet splitting of the s^{th} set, $\delta\Lambda_s$, as the difference between the largest and smallest eigenvalues in the quartet. We also define the inter-quartet gap between the s^{th} and $(s+1)^{\text{th}}$ quartets, $\Delta\Lambda_s$, as the difference between the smallest eigenvalue of the higher quartet and the largest eigenvalue of the lower quartet.

We use the notation $\langle \cdot \rangle_Q$ to denote the expectation value over sub-ensembles with fixed gluonic topological charge $\pm Q$.

Unless otherwise specified, the eigenvalues are expressed in physical units of MeV, with the scale set using the quoted lattice spacing.

IV. SPECTRUM AND INDEX THEOREM

In this section we study the Dirac spectra, and show how the continuum results emerge for the improved operators.

A. The Index Theorem

We begin our analysis by qualitatively comparing the low-lying modes of various staggered quark operators on typical gauge backgrounds selected from those with $Q = 2$. Working at approximately fixed lattice volume

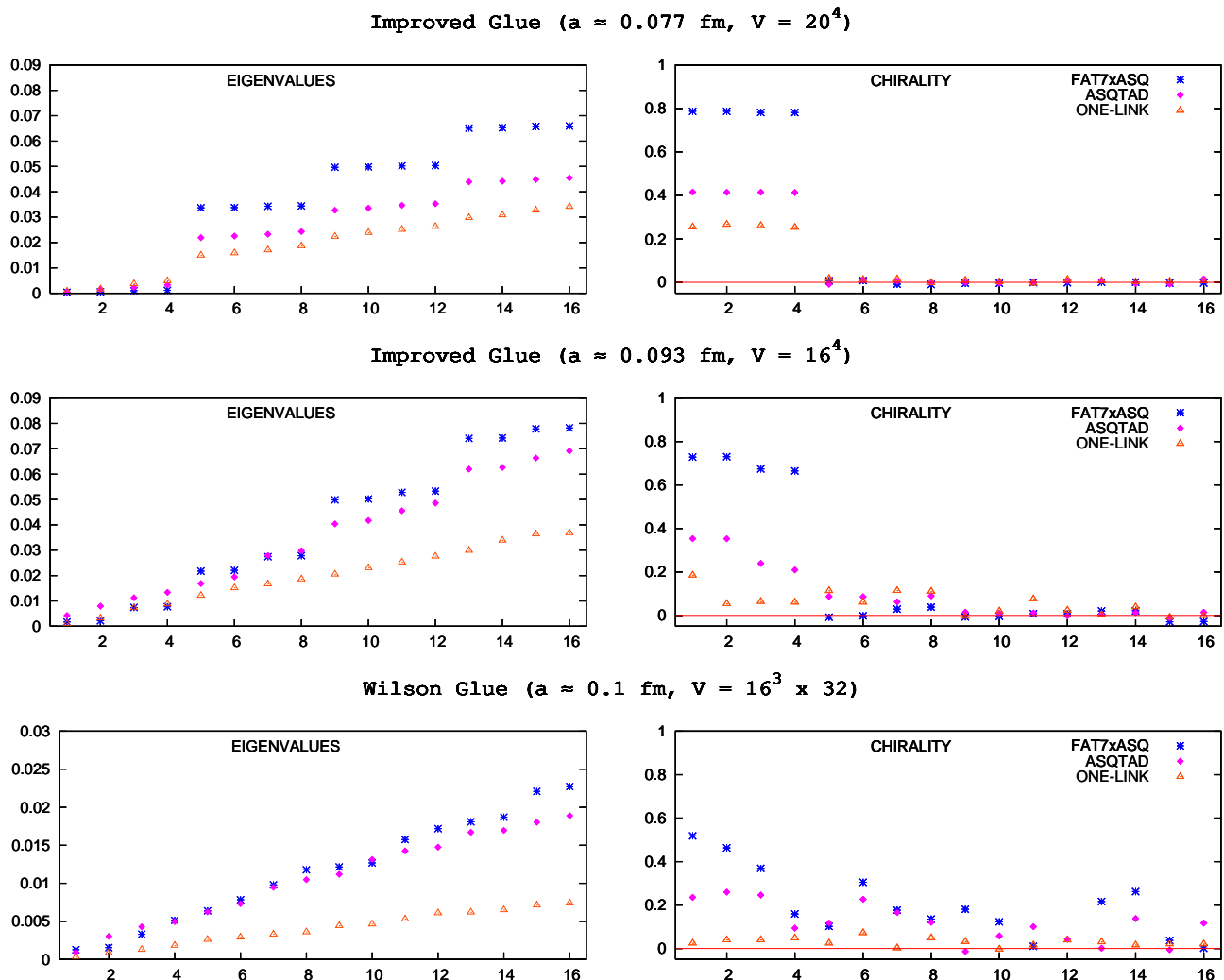


FIG. 2: The positive half of several typical low-lying eigenmode spectra for configurations of $Q = 2$, in lattice units. The x-axis is eigenvalue number. The HYP operator gives results very similar to FAT7xASQ, and they are not shown for clarity.

($aL \approx 1.50$ fm), we compare three different gauge field actions: unimproved Wilson at $a = 0.1$ fm; Symanzik improved, Eq. (23), at a comparable $a = 0.093$ fm, and at the finer $a = 0.077$ fm. In Fig. 2 we show both the value and the chirality of the first sixteen positive eigenvalues.

Near the continuum limit we expect to see first $2|Q| = 4$ near-zero modes with their chirality renormalised slightly away from unity. The remaining modes should have chirality near zero and divide into almost degenerate quartets with intra-quartet splitting much smaller than the inter-quartet gap.

For the improved gauge action on the finer lattice the spectrum looks quite continuum-like for all Dirac operators and we see a clear Index Theorem. For the improved operators we also see a very clear quadruple degeneracy in the non-zero modes. The renormalisation of the chirality away from 1 is small for the improved Dirac operators (around $Z = 1.2$), becoming as large as $Z \approx 4$ for the ONE-LINK fermions. This result is fairly typical

of operator renormalisation for staggered quarks, with the improved actions showing significantly better renormalisation factors [56, 57, 58]. We will discuss later the renormalisation of the chiral condensate and see the same effect.

On the coarser improved gauge background, we still have a good approximation to the Index Theorem using the FAT7xASQ and HYP operators: there is a separation between near-zero modes of high chirality and the rest of the spectrum; the number of near-zero modes is $2|Q|$; and all of them have very similar chiralities. The rest of the spectrum have almost zero chirality and cluster into quartets. These properties can be seen to a lesser extent for the ASQTAD operator, but are absent in the ONE-LINK case.

Nothing clear can be seen in the unimproved, Wilson gauge case. Improving the Dirac operator makes a difference, increasing the chirality of the low modes. Nonetheless the chiralities do not show a clear Index Theorem,

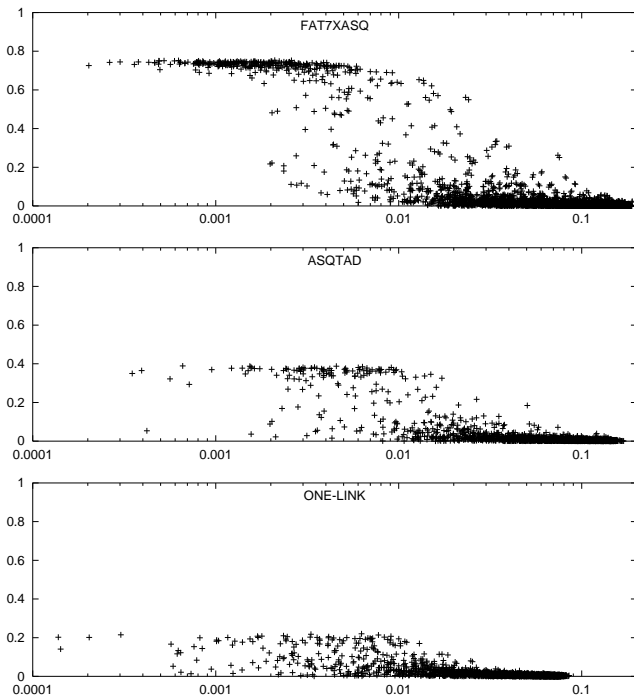


FIG. 3: A scatter plot for different staggered quark formulations, with absolute value of the chirality on the y axis and eigenvalue λ_s on the x axis, in lattice units. The lowest 50 eigenvalues for 147 configurations from our 16^4 , $a=0.093$ fm ensemble are plotted.

and the eigenvalues do not gather into quartets.

To give an idea of the behaviour over a large ensemble, Fig. 3 shows a scatter plot of the absolute value of the chirality versus the (positive) eigenvalues. Results for different operators are plotted, using the same $a = 0.093$ fm ensemble of gauge fields. We can see the formation of a gap between modes of small and large chirality as we improve the staggered operators, as well as the overall increase in chirality of the near-zero modes. As seen in Fig. 4 for the most improved operator on the finest ensemble, the separation gets sharper as we approach the continuum limit.

The separation is not strict even for the most improved action, with a few configurations showing intermediate values of the chirality. At least some of these cases are associated with configurations where the $\mathcal{O}(a^2)$ ambiguity in the topological charge is large and/or where the total number of near-zero modes is greater than the minimum prescribed by the Index Theorem, i.e. $n_+ + n_- > N_t|Q|$.

As the near-zero modes for the more improved actions clearly separate and have well defined chirality, we may define a fermionic index $\bar{Q} = (n_+ - n_-)/N_t$ on each configuration. \bar{Q} is then strongly correlated with Q , and we have a very good approximation to the Index Theorem. We expect the number of configurations where $Q \neq \bar{Q}$ to vary as $\mathcal{O}(a^2)$. Although we don't have enough statistics to test this scaling quantitatively, we can get some esti-

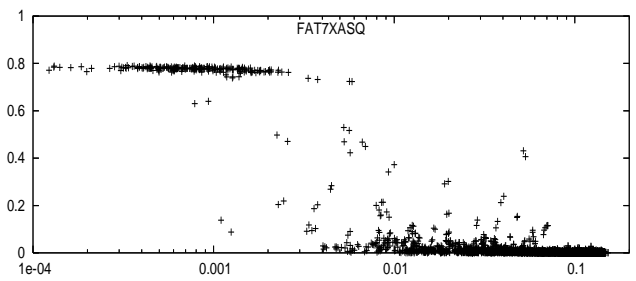


FIG. 4: A scatter plot for FAT7XASQ, with absolute value of the chirality on the y axis and eigenvalue λ_s on the x axis, in lattice units. The lowest 50 eigenvalues for around 100 configurations from our 20^4 , $a = 0.077$ fm ensemble are plotted.

mates from our results. For our $a = 0.093$ fm ensemble, the disagreement between Q and \bar{Q} is around 10%, and it goes down to about 2% on the finest $a = 0.077$ fm ensemble. This ambiguity is therefore of the same order as the one intrinsic in the gluonic definition, as discussed in Sec. III B. We stress here that \bar{Q} played no part in the assignment of configurations into sectors of fixed topological charge.

We may worry that when $Q \neq \bar{Q}$ the division of the eigenvalues into near-zero and non-zero modes, and the division of the latter into quartets, will be skewed. For instance, on such configurations the intra-quartet splitting will be as large as the inter-quartet gap. The examination of the histograms of $\delta\Lambda_s$ and $\Delta\Lambda_s$ show that in all cases any slight bias on the mean is swamped by the statistical spread.

B. The Banks–Casher relation

We begin our quantitative analysis with the Banks–Casher relation (11), which links the density of non-zero eigenvalues at the origin with the chiral condensate, and thus provides a model independent determination of Σ . For N_t degenerate flavours, the Banks-Casher relation would be modified to

$$\Sigma = \pi\rho(0)/N_t. \quad (24)$$

This is the relevant form for staggered fermions, with $N_t = 4$. Note that the appropriate $\bar{\psi}\psi$ operator for the chiral condensate is the taste-singlet, but this is the local operator and so there are no other modifications to the Banks-Casher relation for staggered quarks.

In Fig. 5 we plot a histogram of the spectral density averaged over all configurations in the ensemble. The errors come from a jack-knife analysis of the data.

The spectrum divides clearly into two separate sections: a sharply peaked spike near $\lambda = 0$, coming from the near-zero modes, and a broader distribution at larger eigenvalue from the remaining modes. This separation is much sharper for the improved actions. The spectral den-

TABLE II: Estimates of the cube root of the bare chiral condensate, $\Sigma^{1/3}$, (in units of MeV) from: the Banks-Casher relation (upper section) and comparisons of eigenvalue distributions with random matrix theory (lower section).

		Dirac operator			
a/fm	aL/fm	ONE-LINK	ASQTAD	HYP	FAT7xASQ
0.125	1.50	348 (10)	274 (10)	—	256 (10)
0.093	1.12	330 (30)	—	—	260 (10)
0.093	1.49	349 (10)	275 (10)	279 (10)	260 (10)
0.093	1.86	360 (10)	—	—	255 (10)
0.077	1.54	322 (10)	253 (10)	—	238 (10)
<hr/>					
0.125	1.50	356 (8)	283 (6)	—	260 (6)
0.093	1.12	383 (43)	—	—	289 (33)
0.093	1.49	361 (12)	293 (5)	279 (4)	281 (2)
0.093	1.86	358 (6)	—	—	286 (4)
0.077	1.54	321 (10)	266 (10)	—	256 (5)

sities corresponding to the improved actions also show an excellent scaling behaviour with the lattice spacing.

For larger λ , a λ^3 behaviour is expected to set in. Having only calculated the first 100 eigenvalues, however, we instead find the spectral density cut off at larger λ . It would be necessary to include many more modes to see this behaviour.

Using Eq. (24), we can extract the single taste chiral condensate by extrapolating the density of non-zero modes to zero, $\rho(\lambda) \rightarrow \rho(0)$. The chiral condensate is the order parameter for chiral symmetry breaking, and we see clear evidence from Fig. 5 that all our lattices are large enough that $\Sigma \neq 0$.

To estimate $\rho(0)$ we carry out uncorrelated fits to $\rho(\lambda)$, excluding the near-zero mode peak from the fit range. We use a polynomial fit function

$$\rho(\lambda) = \rho_0 + \lambda\rho_1 + \lambda^2\rho_2 + \lambda^3\rho_3. \quad (25)$$

We carry out a number of fits to each data set, constraining different combinations of ρ_i to zero and varying the fit range. The intercept ρ_0 is then used to obtain the chiral condensate values given in the upper half of Table II. The quoted errors cover the fit function and range uncertainties, which dominate the statistical and fitting errors.

Note that the ONE-LINK density at the origin $\rho(0)$ is much larger than the one for the improved case. This is clearly noticeable when inverting the operator, with the improved actions needing fewer iterations than the ONE-LINK action (also seen in [41]).

The larger $\rho(0)$ gives a much higher value for Σ for the ONE-LINK action, but it is important to note that this is the bare lattice chiral condensate and does not have to agree between actions in the same way that the bare lattice quark mass does not. What should agree is the chiral condensate defined in some physical way, for example in the \overline{MS} scheme at a fixed scale. The appropriate renormalisation factor for $\bar{\psi}\psi$ is the inverse

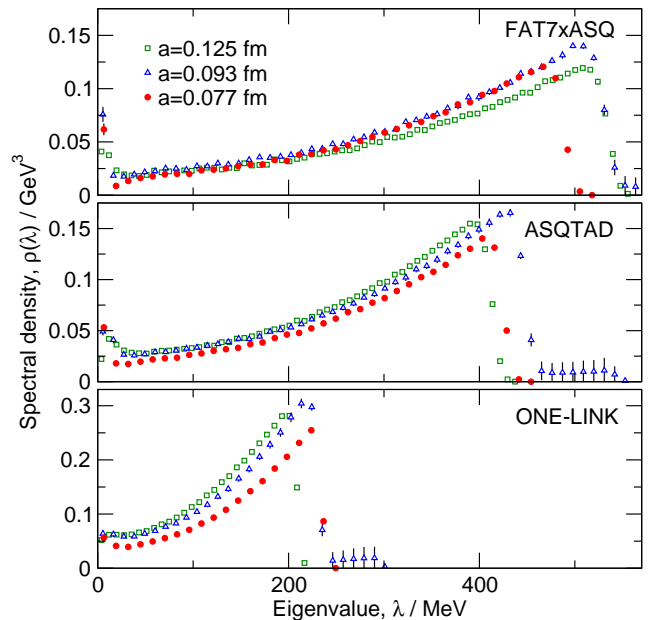


FIG. 5: The spectral density for different Dirac operators at fixed lattice volume $aL = 1.5$ fm. Only the contribution of the first 100 eigenvalues have been calculated.

of that for the quark mass and this has been calculated to $\mathcal{O}(\alpha_s)$ for the staggered quark actions used here and the improved gluon action (at $\mathcal{O}(\alpha_s)$ there is no effect from one-loop improvements to the gluon action or the presence of sea quarks). The quark mass renormalisation was quoted in [59] as:

$$m^{\overline{MS}}(\mu) = \frac{am_0}{a} \left(1 + \alpha_V(q^*) Z_m^{(2)}(a\mu, (am)_0) + \mathcal{O}(\alpha^2) \right),$$

$$Z_m^{(2)}(a\mu, am_0) = \left(b(am_0) - \frac{4}{3\pi} - \frac{2}{\pi} \ln(a\mu) \right). \quad (26)$$

where $b(am_0)$ is the finite piece of the lattice mass renormalisation and has small am_0 dependence. The $\frac{4}{3\pi}$ comes from the continuum mass renormalisation. With tadpole-improvement $b(0)$ takes the value 0.543 for the ASQTAD quark action and 3.6 for the ONE-LINK action (denoted naive staggered quarks in [59]). For FAT7xASQ $b(0)$ is 0.375. For the chiral condensate renormalisation, Z_S we need to take the inverse of the renormalisation above. We take μ to be 2 GeV, as a standard reference point, and take the scale of α_s to be $2/a$, as determined for the ASQTAD action at comparable values of a in [59]. The values of α_s in the V scheme in the quenched approximation are taken from [60]. It is then clear that Z_S for the ASQTAD and FAT7xASQ actions is very close to 1 for all lattice spacing values, but significantly smaller than 1 for the ONE-LINK action. The renormalisation brings the value of the physical chiral condensate for the ONE-LINK action from the Banks-Casher relation down to 290 MeV, much closer to that from the improved actions. The renormalisation constant is so far from 1 in

this case, however, that significant higher order corrections are to be expected. For the improved actions, however, the renormalisation is very small indeed and numbers change by less than 2% from the bare results of table II. The estimated uncertainty from higher order perturbative corrections is 4% i.e. $1 \times \alpha_s^2$. From table II we also have a statistical error of 4%. In addition there are statistical and systematic errors from the determination of the lattice spacing that are relevant here. All of these errors are small compared to the overall 10-20% error from the inability to determine the lattice spacing uniquely in the quenched approximation. This means that any physical value for the chiral condensate that we quote will have a significant error from this source alone. Our results for the FAT7XASQ action give a result for $(-\overline{\psi\psi})^{1/3} \overline{MS}(2\text{GeV})$ of $260(10)(10)(30)$ MeV, where the first error is statistical, the second perturbative and the third a quenching error. This is in agreement with other results in the literature in the quenched approximation (for example, [61]). An improvement on this value requires unquenched configurations, but our result shows that an accurate calculation is certainly possible with improved staggered quarks.

C. Scaling of the near-zero modes

The near-zero eigenvalues for a given Dirac operator vary both with the lattice spacing and volume.

In Fig. 6 we show the variation of the mean near-zero modes $\langle \Lambda_0 \rangle$ with lattice spacing at fixed physical volume ($aL \approx 1.5$ fm). The panels show the results for sectors of topological charge $|Q| = 1$ and 2. For a sufficiently small lattice spacing, we expect the eigenvalues to go to zero as (a^2) plus $\mathcal{O}(a^4)$ corrections. The improved staggered results show this trend across the full range of lattice spacings studied, with small $\mathcal{O}(a^4)$ corrections, slightly positive for FAT7XASQ but negative for ASQTAD. By contrast, the ONE-LINK near-zero modes show very strong deviations from the leading order scaling behaviour.

In almost all quantities that we measure the HYP operator gives results that agree with FAT7XASQ within one standard error. Unless there is a significant difference we do not discuss the HYP data and for clarity they are not shown on the figures, but we have checked that all statements regarding FAT7XASQ apply equally to HYP.

The FAT7XASQ near-zero modes are numerically smaller than those of the ONE-LINK action for $a \lesssim 0.13$ fm. The ASQTAD near-zero modes are smaller than the ONE-LINK ones for $a \lesssim 0.08$ fm. Even when the modes are similarly sized, however, we have seen earlier that there is a qualitative difference in the chirality as we improve the action. This is a clear signal that the operator improvement is working.

The variation of the near-zero eigenvalues with volume at fixed lattice spacing is shown in Fig. 7. $\langle \Lambda_0 \rangle$ is expected to vary as the inverse square root of the volume.

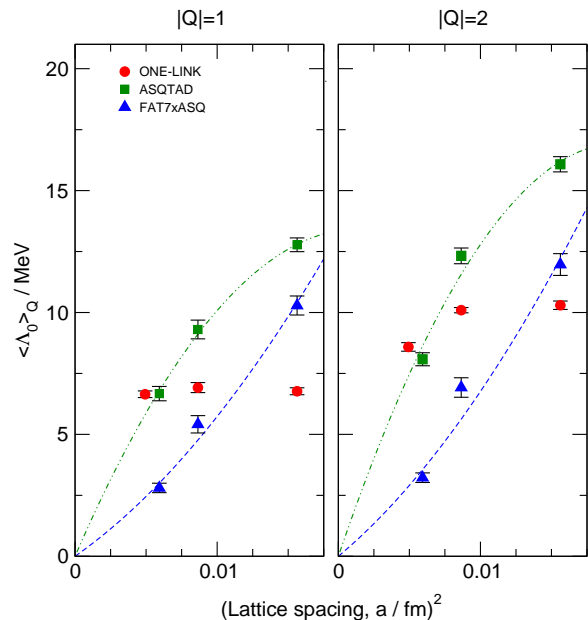


FIG. 6: The scaling of the near-zero modes with lattice spacing at fixed lattice volume for different topological charge sectors. The near-zero modes are averaged. Also shown are linear plus quadratic fits through the origin for ASQTAD and FAT7XASQ.

This can be justified in a semiclassical picture, where the topological charge density is dominated by a dilute gas of instantons. The finite volume corrections to the zero modes come from the lack of large instantons, excluded from the lattice by their cores sizes $r \gtrsim aL$. Such corrections should vary as $1/\rho^2$, or $1/\sqrt{a^4 V}$ [62].

We see from Fig. 7 that the data at fixed lattice spacing follows this approximate volume scaling quite closely. We might ask whether $\langle \Lambda_0 \rangle$ really goes to zero in the large volume limit at finite lattice spacing. Fits to our data allowing a non-zero intercept are not stable, but a large reduction in statistical errors, as well as simulations in larger volumes, would be needed to answer this question definitively.

D. Scaling of the low-lying non-zero modes

We turn now to the low-lying non-zero modes. From the requirement of a physical spectral density in Eq. (10) and the Banks-Casher relation, Eq. (11), it is clear that the size of these is governed, up to a constant, by the product of the bare chiral condensate and the volume ΣV . Specifically, the number of modes in a small interval $(0, \delta)$ should scale as $\sim \delta \rho(0) V \sim \delta \Sigma V$, and therefore we expect each mode to scale as $(\Sigma V)^{-1}$. The variation of these modes with changing lattice spacing and volume is therefore fixed by the response of the bare chiral condensate.

In Fig. 8 we show the variation of the first two non-

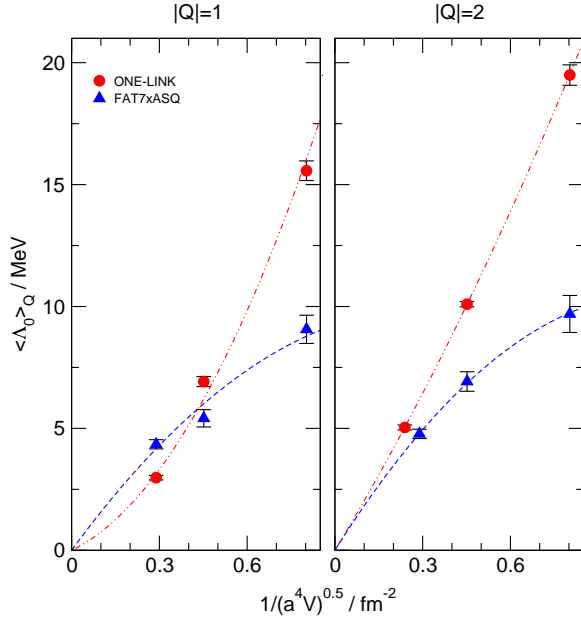


FIG. 7: The averaged near-zero modes as a function of lattice volume at $a = 0.093$ fm for different topological charge sectors. Also shown are linear plus quadratic fits through the origin.

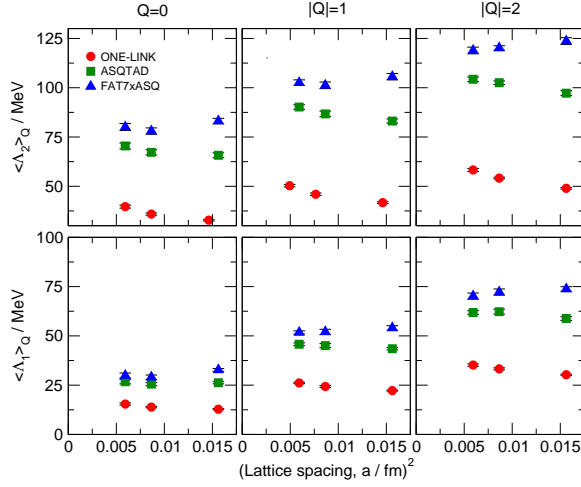


FIG. 8: The scaling of the non-zero modes with lattice spacing at fixed lattice volume for different topological charge sectors. In each case the quartets are averaged.

zero mode quartets $\langle \Lambda_{1,2} \rangle$ with lattice spacing at fixed physical volume ($aL \approx 1.5$ fm) for several Q . For all the improved actions the changes are very small, indicating only small discretization errors, as for the chiral condensate. For the near-zero modes, the deviations from the leading order scaling behaviour seem to be of opposite sign for ASQTAD and FAT7xASQ. The ONE-LINK data show much larger deviations, of the same sign as for the ASQTAD data.

The different actions appear to lack a common continuum limit. This is not surprising: as discussed above,

the plot is inversely related to the density and therefore the bare chiral condensate. As explained earlier, this receives a large renormalisation for the ONE-LINK action compared to the improved actions that means that the bare results are not comparable.

From the arguments above, we expect $\langle \Lambda_s \rangle$ to vary as the inverse volume at fixed lattice spacing. We find this to be so for both ONE-LINK and improved actions. Fig. 9 shows the results for $s = 1, 2$.

Given the different volume scaling of the two sets of eigenmodes, we cannot really talk about a gap between near-zero and non-zero modes: we can always choose a volume large enough that the “non-zero” modes (suppressed as $1/V$) are numerically smaller than the “near-zero” modes (which fall only as $1/\sqrt{V}$). The modes are still qualitatively different however, and can be separated by their chirality.

Taste breaking interactions disappear in the continuum limit and the eigenmodes should recover a 4-fold degeneracy. We plot the intra-quartet splitting of the first quartet, $\langle \delta \Lambda_1 \rangle$ for different sectors of topological charge in Fig. 10 (higher quartets have smaller splittings). The lattice volume is fixed at $aL \approx 1.5$ fm. The splitting falls with lattice spacing, as expected, and in a way consistent with the $\mathcal{O}(a^2)$ dependence of the taste breaking interactions. The splitting depends only weakly on the topological charge.

This is the only quantity we have studied where there is a difference of more than one standard error between HYP and FAT7xASQ results; the FAT7xASQ results are marginally closer to our continuum expectations. (This was also true in Fig. 6, but the difference was not statistically significant).

There are strong similarities between this plot and Fig. 6: the improved fermion actions all show only very

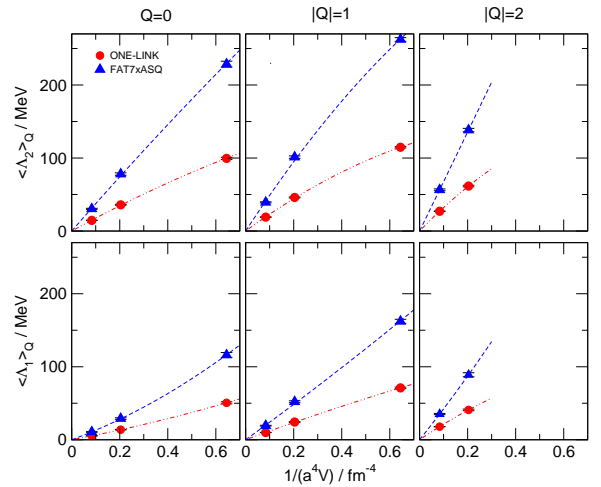


FIG. 9: The scaling of the non-zero modes with volume at fixed lattice spacing for different topological charge sectors. In each case the quartets are averaged. Also shown are linear plus quadratic fits through the origin.

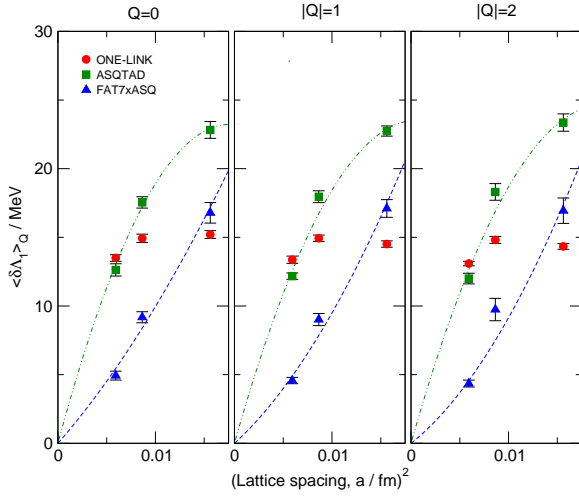


FIG. 10: The scaling of the first non-zero intra-quartet splitting with lattice spacing at fixed lattice volume in different topological charge sectors. Higher quartets have smaller splittings. The lines are linear plus quadratic fits for ASQTAD and FAT7XASQ .

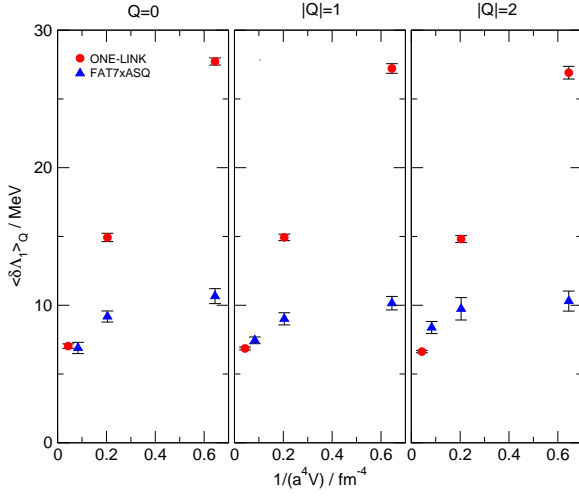


FIG. 11: The scaling of the first non-zero intra-quartet splitting with volume at fixed lattice spacing in different topological charge sectors. Higher quartets have smaller splittings. See comments in Fig. 6.

weak deviations from the naive scaling behaviour; the $\mathcal{O}(a^4)$ corrections are positive for FAT7XASQ and negative for ASQTAD; the ONE-LINK results however show very large deviations from the expected behaviour. Numerically, the FAT7XASQ splittings are smaller than the ONE-LINK for $a \lesssim 0.12$ fm; the ASQTAD numbers are less for $a \lesssim 0.08$ fm.

In Fig. 11 we show the variation of the splitting with volume at fixed lattice spacing. Once more the splitting is independent of the topological charge. There is a striking difference in the volume dependence: the ONE-LINK splittings vary markedly whilst the improved action results are nearly insensitive.

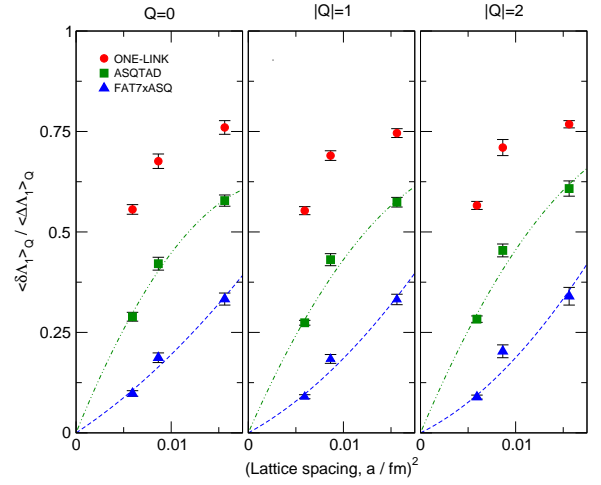


FIG. 12: The ratio of the intra-quartet splitting of the first non-zero quartet to the inter-quartet gap between first and second quartets as a function of lattice spacing at fixed lattice size $aL \approx 1.5$ fm. The lines are linear plus quadratic fits for ASQTAD and FAT7XASQ .

To satisfy ourselves that there is a clear restoration of the taste symmetry, we need the intra-quartet splitting $\langle \delta\Lambda_s \rangle$ to be much less than the gap between neighbouring quartets $\langle \Delta\Lambda_s \rangle$. In Fig. 12 we show the ratio of these as a function of lattice spacing for $s = 1$ (where it is largest).

Again, the ratios show little dependence on the topological charge. In all cases the improved action results are better than the ONE-LINK. This is increasingly true at small lattice spacings, as the improved actions show a ratio falling clearly to zero as a^2 .

We can understand these results quite easily. As the quartets become degenerate, $\langle \Delta\Lambda_s \rangle$ will tend towards the difference between the quartet means. Fig. 8 shows this is controlled by the chiral condensate and has little lattice spacing dependence for the improved actions. The intra-quartet splitting falls as a^2 and so, therefore, will the ratio.

V. RMT PREDICTIONS

As discussed previously, the chiral symmetries of staggered quarks are more complicated than for continuum QCD. At finite lattice spacing the $N_t^2 = 16$ pions split into 5 multiplets containing (1, 4, 6, 4, 1) states, and only one of these states becomes massless in the chiral limit. This is known as the “Goldstone pion”, with mass M_G . The fifteen remaining states have masses M_{NG} arising from the taste breaking interactions. The (chirally extrapolated) masses are $\mathcal{O}(a^2)$ and therefore zero only in the continuum limit.

There are potentially *two* universal regions for different

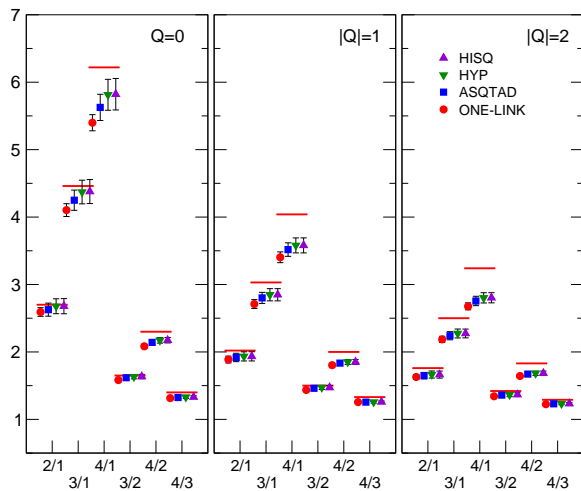


FIG. 13: The ratios of expectation values of small eigenvalues for the $aL = 1.5$ fm, $a = 0.093$ fm ensemble for different Dirac operators, compared with the predictions based on a universal distribution (horizontal lines) for $|Q| \leq 2$.

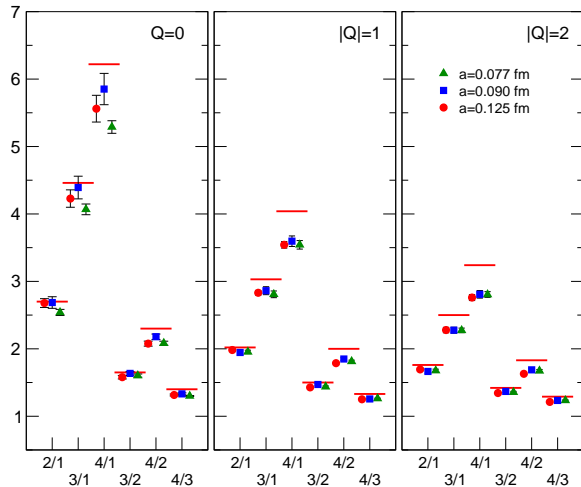


FIG. 14: The ratios of expectation values of small eigenvalues for the $aL = 1.5$ fm ensembles for the FAT7XASQ operator compared with the predictions based on a universal distribution (horizontal lines) for $|Q| \leq 2$.

parameters of the system:

$$\begin{aligned} \varepsilon\text{-regime:} & \quad (\Lambda_{\text{QCD}})^{-1} \ll L \ll (M_{\text{NG}})^{-1}, \\ \varepsilon'\text{-regime:} & \quad (M_{\text{NG}})^{-1} \ll L \ll (M_{\text{G}})^{-1}. \end{aligned}$$

The first corresponds to Eq. (12), with the same chiral symmetries that we expect in the continuum. The low-lying non-zero modes have a near N_t -fold degeneracy, and follow the predictions of Eqs. (14,15). These are *exactly the same* distributions as for continuum QCD (and chiral lattice fermions [63, 64, 65, 66, 67, 68]).

At finite lattice spacing there is a second, ε' -regime, where the finite volume partition function describes only the static mode of the single Goldstone pion. There is not

even approximate restoration of the continuum symmetries, and the associated RMT has only $U(1) \otimes U(1)$ chiral symmetry. The universal predictions for the eigenvalues are therefore strikingly different from those for continuum QCD. In particular, the predictions are the same for all sectors of topological charge [69]. Presumably it is this regime that was studied in [21, 22, 23, 24, 25]. With the coarse lattices and unimproved gauge ensembles used in these studies, they observed no sensitivity of the eigenvalue spectra to Q , leading to the incorrect folklore that staggered quarks are “blind to the topology”.

To see the continuum chiral symmetries, there must be a sufficiently large mass gap between the heaviest pion and the lightest of the other hadrons. This requires the use of improved gauge and fermion actions and a sufficiently small lattice spacing. In particular if we increase the size of the lattice L , the lattice spacing must be reduced accordingly in order to satisfy $L \ll (M_{\text{NG}})^{-1}$. Otherwise we would start to see the effects of the mass of the non-Goldstone pions. At coarse lattice spacings, with unimproved fermions, $M_{\text{NG}} \approx \Lambda_{\text{QCD}}$ and there will be no ε -regime.

If the lattice spacing is kept fixed and we increase the volume, we expect there will be a non-universal crossover until the lattice reaches the ε' -regime when universal behaviour will resume. Of course, it would be interesting to simulate a range of lattice sizes and witness the crossover between the two universal regions. The range of lattice spacings is, however, well beyond the resources of this study. We instead concentrate on the continuum-like region.

A. Comparison

We begin by comparing the ratios of the mean non-zero eigenvalues $\langle \Lambda_s \rangle_Q / \langle \Lambda_t \rangle_Q$ (which we denote “s/t”) to the ratios from RMT. Factors of the chiral condensate scale away, so this provides a parameter-free test of the ε -regime predictions.

We show the eigenvalue ratios in Figs. 13-15. The ratios differ markedly between different topological charge sectors, showing clearly that the staggered fermions are in no way “topology blind”. Also shown are the ratios predicted by RMT. Fig. 13 shows that all the staggered actions agree quite well with the expected ratios at $a = 0.093$ fm. We therefore have good evidence for the existence of a continuum ε -regime. It also implies that the continuum chiral symmetries are present, with the correct pattern of spontaneous breaking.

There are some deviations from the universal predictions. They are not discretization effects: Fig. 14 shows the FAT7XASQ ratios for a range of different lattice spacings at fixed volume $aL \approx 1.5$ fm and discrepancies exist even on the finest lattice. Increasing the system size from 1.5 to 1.8 fm in Fig. 15 does reduce the size of the disagreement. Indeed, on the larger volume the ratios agree with RMT at least as well as for chiral fermions on com-

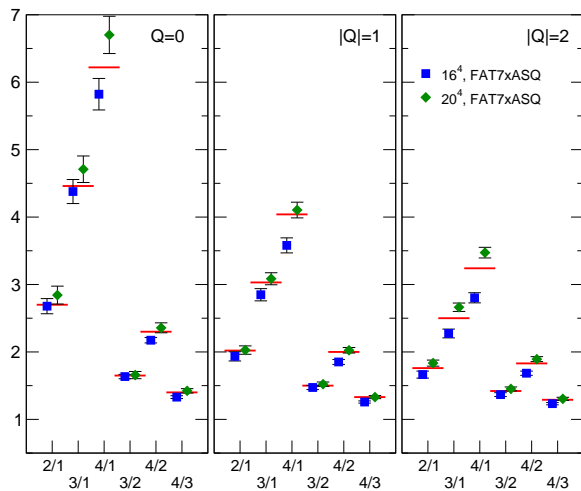


FIG. 15: The ratios of expectation values of small eigenvalues of the FAT7xASQ operator for two $a = 0.093$ fm ensembles of different volumes compared with the predictions based on a universal distribution (horizontal lines) for $|Q| \leq 2$.

parable lattices [68].

Fig. 13 appears to suggest that the ONE-LINK Dirac operator fits the universal predictions as well as the improved operators. This appears so even on the coarsest lattices despite the large pion splitting and lack of obvious spectral quartets in the ONE-LINK spectrum.

In this respect the “ratios plots” can be misleading. Firstly they only compare the mean eigenvalues with RMT and provide no information as to whether the shape of the individual distributions match. Also, when comparing with RMT we must rescale all the eigenvalues using the chiral condensate. Agreement with the ratio plot does not imply that eigenvalues in different topological charge sectors are scaled by the same factor.

To address the first point we separately fit the individual spectral densities to the predictions from RMT. These one parameter fits based on Eq. (13) yield a prediction for the chiral condensate. To avoid the ambiguities of histogram bin-size we use the cumulative eigenvalue distributions,

$$p(\lambda) = \int_0^\lambda d\lambda' \rho(\lambda'). \quad (27)$$

We show examples of the fits in Figs. 16 and 17.

For all operators the fits are worst for low s and for small $|Q|$. We can qualitatively understand this in terms of eigenvalue repulsion. The taste changing interactions have split the near-zero modes, which has a knock-on effect on the rest of the spectrum as the eigenvalues avoid level crossings. The lower quartets are closest to the near-zero modes and are thus most strongly affected. As the quartets get numerically larger as we increase the topological charge, so the repulsion should be less.

It is clear that the improved Dirac operators match the predictions of RMT very closely over the full range

of lattice spacings. By contrast, even at $a = 0.077$ fm the ONE-LINK Dirac operator still shows significant discrepancies.

Separately fitting the ($Q = 0, k = 1.4$) and ($|Q| = 0.3, k = 1$) eigenvalue distributions to the RMT predictions gives 7 values for the bare chiral condensate for each Dirac operator on each ensemble. We find these numbers to be broadly consistent. The spread in the numbers is greatest for the ONE-LINK action and on the smallest volumes. This is not surprising, when such eigenvalue distributions showed the greatest deviation from the RMT predictions

The lower half of Table II gives estimates for the chiral condensate obtained from the median of the seven individual numbers. The quoted errors are half the range, which forms the dominant uncertainty.

We can compare these with the model-independent estimates of Σ obtained using the Banks–Casher relation. There is very good agreement between the numbers. The dominant source of error is different in each case: for the Banks-Casher relation it comes from the choice of fit range and function used to extrapolate the spectral density to zero eigenvalue. For the RMT comparisons, it comes from the variation in fit parameters for different eigenvalues, and is therefore related to exactly how well the effective partition function describes the lattice theory. The good agreement of the numbers suggests both systematic biases are under control. See section IV B for a discussion of how the bare chiral condensate must be renormalised to extract a physical result.

VI. CONCLUSIONS AND OUTLOOK

It is widely believed that any “problems” with a given lattice Dirac operator will show themselves most clearly in the topologically sensitive, low-lying eigenmodes. In this study we have studied these modes for the staggered lattice Dirac operator, using a range of improved and unimproved versions. The improved operators pass all the tests. In particular, and contrary to previous accepted wisdom, such fermions do respond exactly as expected to the gluonic topological charge, and in a way identical to continuum QCD and other lattice formulations of the Dirac operator.

We have seen that for improved operators the eigenvalue spectrum divides cleanly into near-zero and non-zero modes. The near-zero modes are characterised by a uniformly high chirality, with their relative number fixed by the Atiyah-Singer Index Theorem. Indeed they could be used to define the topological charge Q of a configuration. Their eigenvalues scale with lattice spacing and volume as expected.

The non-zero modes, by contrast, have chirality that is near zero. They divide into near degenerate quartets, with the splitting reducing to zero as a^2 in common with the taste breaking interactions. The quartet means are controlled by the chiral condensate and scale with lattice

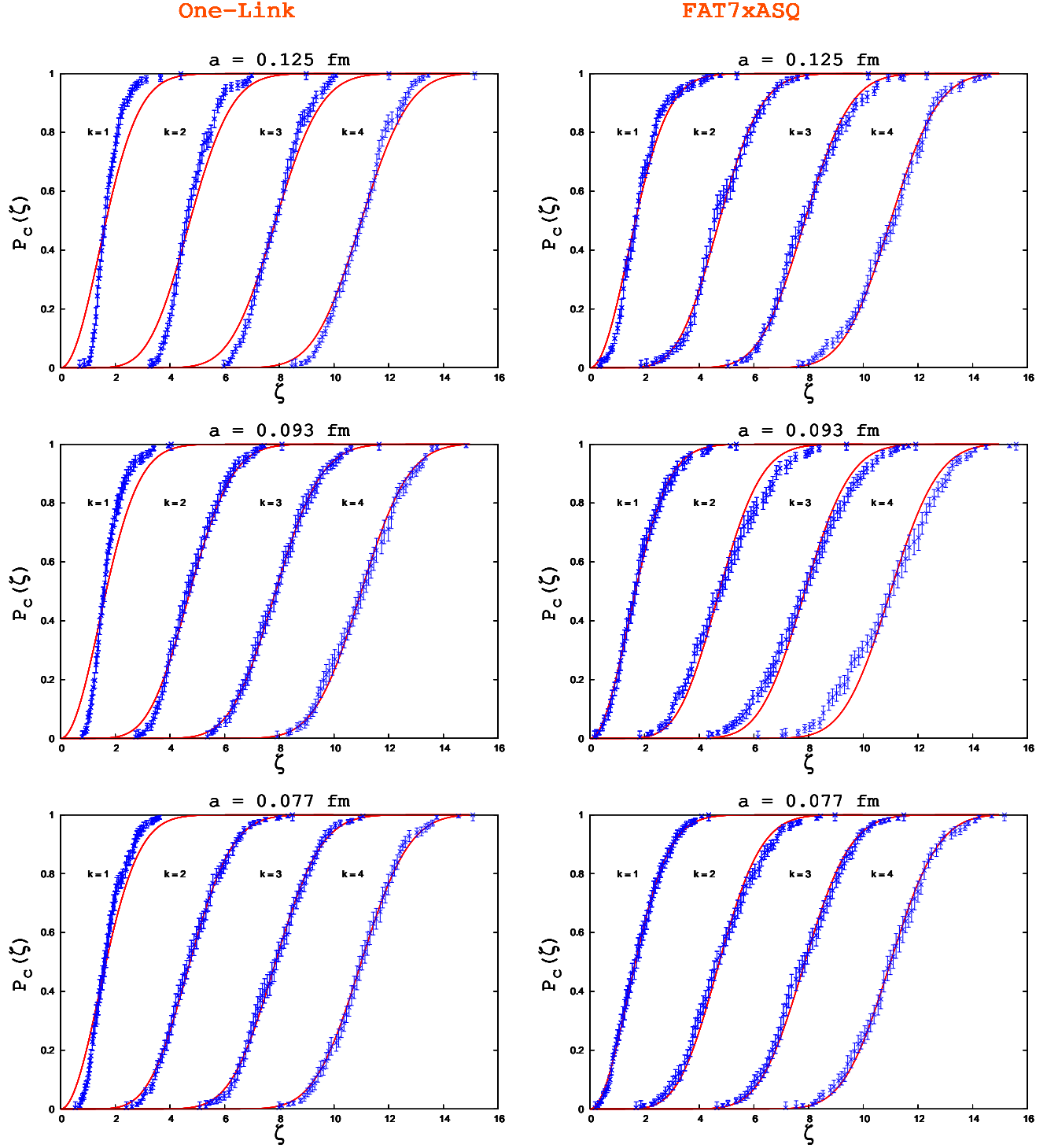


FIG. 16: Comparison of the unfolded eigenvalue distribution with RMT for the lowest eigenvalues in the $Q = 0$ sector. The lattice size is kept at $aL \approx 1.5$ fm

spacing and volume accordingly. In addition, the low-lying non-zero modes follow closely the universal distributions predicted by random matrix theory.

Since the near-zero and non-zero modes scale differently with the volume, it is clear that the “gap” between

the highest near-zero and the lowest non-zero modes is a volume dependent quantity. At finite lattice spacing we can always go to a volume large enough that the two sets of eigenvalues have comparable magnitude. This is not really an issue because the gap is not a physically observ-

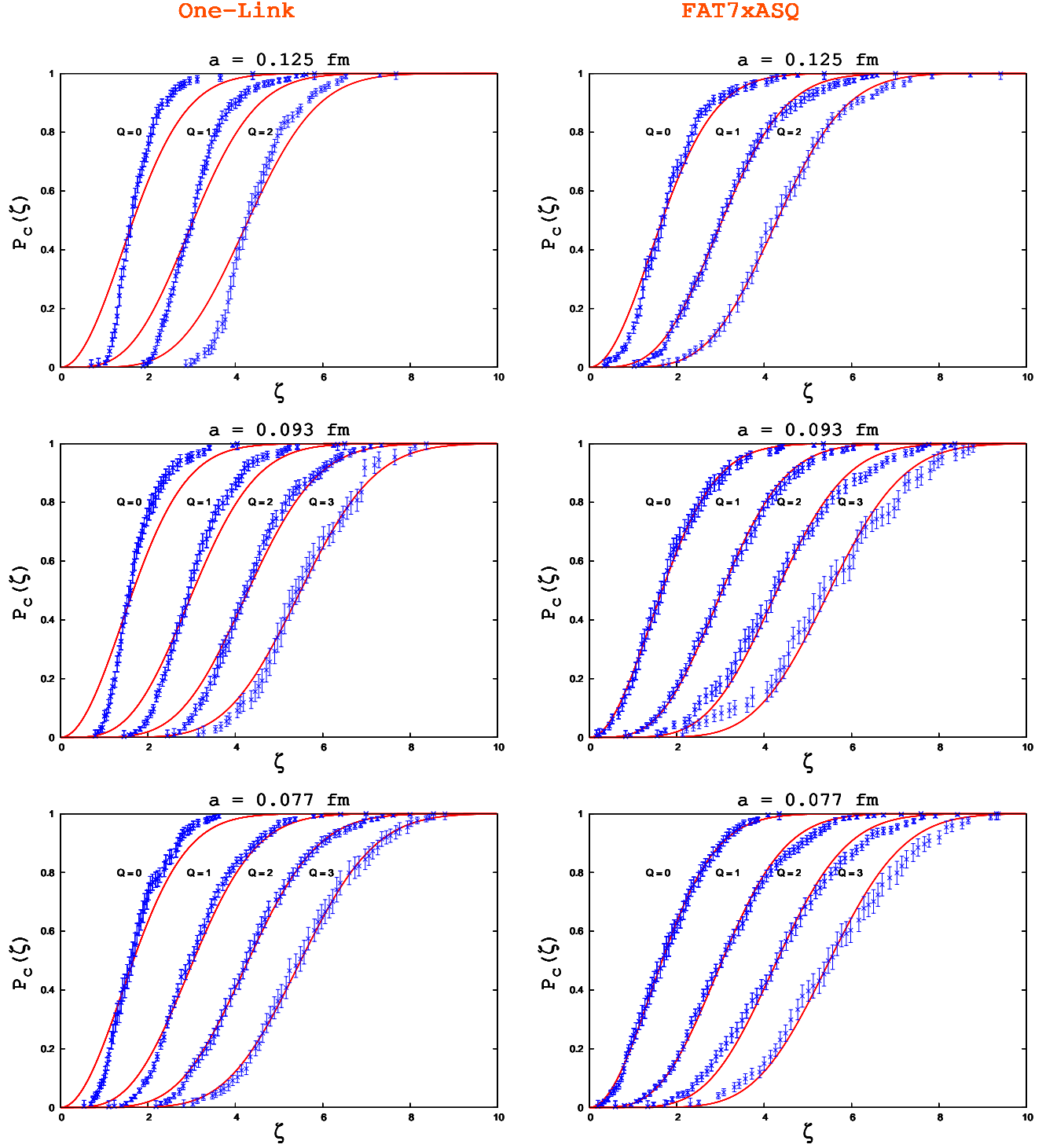


FIG. 17: Comparison of the unfolded eigenvalue distribution with RMT for the lowest eigenvalue for different topological charges. The lattice size is kept at $aL \approx 1.5$ fm

able quantity: what matters is the size of the near-zero modes compared to the light quark masses and whether there is a well-defined Index Theorem. As we have seen the two sets of modes are distinguishable by their chirality, even in the large volume limit.

A quantitative study of axial anomaly physics will require the near-zero modes to be smaller than the light quark masses, i.e. $\lambda < \mathcal{O}(5\text{MeV})$, or, at least, smaller than the sea and valence quark masses used in the simulation. Then the eigenvalue spectrum is cut off at the low

end by the quark mass and the fact that the near-zero modes are not actually zero is irrelevant.

To understand what this means for our quenched ensembles, it is necessary to define the size of the typical near-zero mode. The mean zero mode $\langle \lambda_0 \rangle_Q$ increases as we increase Q , due to eigenvalue repulsion. For our $\beta = 4.8$, $L = 20$ lattice we find that the mean zero-mode is fitted quite well by $\langle \lambda_0 \rangle_Q \approx (3 + Q)$ MeV for $Q = 1.3$. If we define the typical topological charge \bar{Q} to be the RMS value from the topological susceptibility, $\bar{Q} = \sqrt{\chi V} = 2.6$, then the typical near-zero mode is $\bar{\lambda}_0 = (3 + 2.6) \approx 6$ MeV. This suggests that we are already able to study the quenched axial anomaly.

We can attempt to extrapolate our quenched results to ask whether this condition is true on existing configurations from the MILC collaboration [70]. This requires various unsupported, if reasonable, assumptions, not least that sea quark effects do not strongly affect the size of individual near-zero modes and that $\langle \lambda_0 \rangle_Q$ continues to be linear in Q .

Typical dynamical simulation volumes are larger than we have used in this quenched study, to avoid finite volume effects in hadron spectroscopy. As well as an overall \sqrt{V} suppression in the size of the near-zero modes, this will also affect the typical value \bar{Q} and therefore the amount of eigenvalue repulsion. There are two competing effects: the sea quark induced screening of topological charge reduces χ , whilst the larger volume increases the width of the histogram of Q .

Consider the $a = 0.09$ fm MILC ensemble with sea quark masses $m_s/m_{u,d} = 5$ and volume $V = 28^3 \times 96$. Using the data in [28], we obtain $\bar{Q} = 7.3$. Assuming the quenched relation above holds, we have $\bar{\lambda}_0 = (3 + 7.3)/\sqrt{28^4/20^4} \sim 6$ MeV (to be conservative we assume that the volume scaling of the near-zero modes goes with the smallest length of the lattice, therefore 28^4 instead of $28^3 \times 96$). This is very encouraging. The lightest sea quark mass presently used in these dynamical simulations is $m_0 = 16$ MeV, which is several times larger

than this projected near-zero mode.

Even given the caveats surrounding this rough estimate, it does seem likely that a systematic study of the QCD axial anomaly is possible on these configurations and various aspects of this work are now in progress.

An on-going debate surrounds the theoretical justification of the methods use to simulate $N_f < N_t$ flavours of sea quarks [71, 72, 73]. Recent work suggests there is no ambiguity [74, 75, 76]. Our results (and related work elsewhere [35, 37]) indicates that with improved staggered quarks the spectrum matches very closely the continuum expectations with clear restoration of taste symmetry. It therefore paves the way for the full analysis of the staggered taste basis that is necessary to finally resolve this issue.

To clarify the role of topology and the issue of the ε -regime for staggered quarks is important because improved staggered fermions are currently the only lattice formulation that offers the prospect of a comprehensive study of the QCD axial anomaly free from the systematic effects of lattice spacing and unphysically large sea quark mass.

Acknowledgments

This research is part of the EU integrated infrastructure initiative hadron physics project under contract number RII3-CT-2004-506078.

We thank: Ph. de Forcrand for his topological charge measurement code; A. Hasenfratz for help in implementing the HYP operator; G.P. Lepage, P. Damgaard and G. Akemann for useful discussions. E.F., C.T.H.D. and Q.M. are supported by PPARC and A.H. by the U.K. Royal Society. The eigenvalue calculations were carried out on computer clusters at Scotgrid and the Dallas Southern Methodist University. We thank David Martin and Kent Hornbostel for assistance.

-
- [1] E. Follana, A. Hart and C. T. H. Davies, Phys. Rev. Lett. **93**, 241601 (2004), [hep-lat/0406010].
 - [2] E. Follana, Nucl. Phys. Proc. Suppl. **140**, 141 (2005), [hep-lat/0409062].
 - [3] K. Y. Wong and R. M. Woloshyn, hep-lat/0407003.
 - [4] K. Y. Wong and R. M. Woloshyn, Phys. Rev. **D71** (2005), [hep-lat/0412001].
 - [5] M. Atiyah and I. Singer, Bull. Amer. Math. Soc. **69**, 422 (1963).
 - [6] M. Atiyah and I. Singer, Ann. Math. **87**, 596 (1968).
 - [7] P. H. Damgaard, Nucl. Phys. Proc. Suppl. **106**, 29 (2002), [hep-lat/0110192].
 - [8] G. Akemann and P. H. Damgaard, Phys. Lett. **B583**, 199 (2004), [hep-th/0311171].
 - [9] H. Leutwyler and A. Smilga, Phys. Rev. **D46**, 5607 (1992).
 - [10] E. V. Shuryak and J. J. M. Verbaarschot, Nucl. Phys. **A560**, 306 (1993), [hep-th/9212088].
 - [11] S. M. Nishigaki, P. H. Damgaard and T. Wettig, Phys. Rev. **D58**, 087704 (1998), [hep-th/9803007].
 - [12] P. H. Damgaard and S. M. Nishigaki, Phys. Rev. **D63**, 045012 (2001), [hep-th/0006111], see corrections at hep-th/0006111v2.
 - [13] J. J. M. Verbaarschot and I. Zahed, Phys. Rev. Lett. **70**, 3852 (1993), [hep-th/9303012].
 - [14] P. Forrester, Nucl. Phys. B **402**, 709 (1993).
 - [15] M. Golterman and J. Smit, Nucl. Phys. **B245**, 61 (1984).
 - [16] J. Smit and J. C. Vink, Nucl. Phys. **B286**, 485 (1987).
 - [17] S. J. Hands and M. Teper, Nucl. Phys. **B347**, 819 (1990).
 - [18] L. Venkataraman and G. Kilcup, Nucl. Phys. Proc. Suppl. **63**, 826 (1998), [hep-lat/9710086].
 - [19] A. Hasenfratz, "How good is the HYP staggered ac-

- tion?", Talk presented at Lattice 2003 (Tsukuba, Japan).
- [20] E. Follana *et al.*, Nucl. Phys. Proc. Suppl. **129**, 384 (2004).
- [21] M. E. Berbenni-Bitsch, S. Meyer, A. Schafer, J. J. M. Verbaarschot and T. Wettig, Phys. Rev. Lett. **80**, 1146 (1998), [hep-lat/9704018].
- [22] P. H. Damgaard, U. M. Heller and A. Krasnitz, Phys. Lett. **B445**, 366 (1999), [hep-lat/9810060].
- [23] M. Gockeler, H. Hehl, P. E. L. Rakow, A. Schafer and T. Wettig, Phys. Rev. **D59**, 094503 (1999), [hep-lat/9811018].
- [24] P. H. Damgaard, U. M. Heller, R. Niclasen and K. Rummukainen, Phys. Rev. **D61**, 014501 (2000), [hep-lat/9907019].
- [25] P. H. Damgaard, U. M. Heller, R. Niclasen and K. Rummukainen, Phys. Lett. **B495**, 263 (2000), [hep-lat/0007041].
- [26] A. Hasenfratz, Phys. Rev. **D64**, 074503 (2001), [hep-lat/0104015].
- [27] MILC, C. Bernard *et al.*, Nucl. Phys. Proc. Suppl. **119**, 991 (2003), [hep-lat/0209050].
- [28] MILC, C. Bernard *et al.*, Phys. Rev. **D68**, 114501 (2003), [hep-lat/0308019].
- [29] MILC, C. Aubin *et al.*, hep-lat/0409051.
- [30] J. B. Kogut, D. K. Sinclair and M. Teper, Nucl. Phys. **B348**, 178 (1991).
- [31] HEMCGC, K. M. Bitar *et al.*, Phys. Rev. **D44**, 2090 (1991).
- [32] Y. Kuramashi, M. Fukugita, H. Mino, M. Okawa and A. Ukawa, Phys. Lett. **B313**, 425 (1993).
- [33] B. Alles, M. D'Elia and A. Di Giacomo, Phys. Lett. **B483**, 139 (2000), [hep-lat/0004020].
- [34] S. Durr and C. Hoelbling, Phys. Rev. **D69**, 034503 (2004), [hep-lat/0311002].
- [35] S. Durr, C. Hoelbling and U. Wenger, Phys. Rev. **D70**, 094502 (2004), [hep-lat/0406027].
- [36] S. Durr and C. Hoelbling, hep-lat/0408039.
- [37] S. Durr, C. Hoelbling and U. Wenger, hep-lat/0409108.
- [38] S. Durr and C. Hoelbling, Phys. Rev. **D71**, 054501 (2005), [hep-lat/0411022].
- [39] G. P. Lepage, Phys. Rev. **D59**, 074502 (1999), [hep-lat/9809157].
- [40] MILC, C. W. Bernard *et al.*, Phys. Rev. **D61**, 111502 (2000), [hep-lat/9912018].
- [41] MILC, K. Orginos, D. Toussaint and R. L. Sugar, Phys. Rev. **D60**, 054503 (1999), [hep-lat/9903032].
- [42] S. Naik, Nucl. Phys. **B316**, 238 (1989).
- [43] F. Knechtli and A. Hasenfratz, Phys. Rev. **D63**, 114502 (2001), [hep-lat/0012022].
- [44] E. Follana *et al.*, Further improvements to staggered quarks on the lattice, in preparation.
- [45] G. Curci, P. Menotti and G. Paffuti, Phys. Lett. **B130**, 205 (1983).
- [46] **Erratum:**, G. Curci, P. Menotti and G. Paffuti, Phys. Lett. **B135**, 516 (1984).
- [47] M. Luscher and P. Weisz, Commun. Math. Phys. **97**, 59 (1985).
- [48] **Erratum:**, M. Luscher and P. Weisz, Commun. Math. Phys. **98**, 433 (1985).
- [49] M. Alford, W. Dimm, G. Lepage, G. Hockney and P. Mackenzie, Phys. Lett. **B361**, 87 (1995), [hep-lat/9507010].
- [50] F. D. R. Bonnet, D. B. Leinweber, A. G. Williams and J. M. Zanotti, Phys. Rev. **D65**, 114510 (2002), [hep-lat/0106023].
- [51] J. B. Zhang *et al.*, Phys. Rev. **D65**, 074510 (2002), [hep-lat/0111060].
- [52] HPQCD, C. T. H. Davies *et al.*, Phys. Rev. Lett. **92**, 022001 (2004), [hep-lat/0304004].
- [53] P. de Forcrand, M. Garcia Perez and I.-O. Stamatescu, Nucl. Phys. Proc. Suppl. **47**, 777 (1996), [hep-lat/9509064].
- [54] P. de Forcrand, M. Garcia Perez and I.-O. Stamatescu, Nucl. Phys. **B499**, 409 (1997), [hep-lat/9701012].
- [55] J. Cullum and R. A. Willoughby, *Lanczos Algorithms for Large Symmetric Eigenvalue Computations. Vol 1, theory* (SIAM Society for Industrial & Applied Mathematics, Philadelphia, 2002).
- [56] J. Hein, Q. Mason, G. Lepage and H. Trotter, Nucl. Phys. Proc. Suppl. **106** (2002), [hep-lat/0110045].
- [57] H. Trotter, G. Lepage, P. Mackenzie, Q. Mason and M. Nobes, Nucl. Phys. Proc. Suppl. **106** (2002), [hep-lat/0110147].
- [58] W. Lee and S. Sharpe, Phys. Rev. **D66**, 114501 (2002), [hep-lat/0208018].
- [59] C. Aubin *et al.*, Phys. Rev. **D70**, 031504 (2004), [hep-lat/0405022].
- [60] HPQCD and UKQCD, Q. Mason *et al.*, Phys. Rev. Lett., in press, [hep-lat/0503005].
- [61] L. Giusti, F. Rapuano, M. Talevi and A. Vladikas, Nucl. Phys. **B538**, 249 (1999), [hep-lat/9807014].
- [62] UKQCD, D. A. Smith and M. J. Teper, Phys. Rev. **D58**, 014505 (1998), [hep-lat/9801008].
- [63] R. G. Edwards, U. M. Heller, J. E. Kiskis and R. Narayanan, Phys. Rev. Lett. **82**, 4188 (1999), [hep-th/9902117].
- [64] R. G. Edwards, U. M. Heller, J. E. Kiskis and R. Narayanan, Phys. Rev. **D61**, 074504 (2000), [hep-lat/9910041].
- [65] P. H. Damgaard, R. G. Edwards, U. M. Heller and R. Narayanan, Phys. Rev. **D61**, 094503 (2000), [hep-lat/9907016].
- [66] P. Hasenfratz, S. Hauswirth, T. Jorg, F. Niedermayer and K. Holland, Nucl. Phys. **B643**, 280 (2002), [hep-lat/0205010].
- [67] W. Bietenholz, K. Jansen and S. Shcheredin, JHEP **07**, 033 (2003), [hep-lat/0306022].
- [68] L. Giusti, M. Luscher, P. Weisz and H. Wittig, JHEP **11**, 023 (2003), [hep-lat/0309189].
- [69] P. H. Damgaard, private communication, 2004.
- [70] C. Aubin *et al.*, hep-lat/0402030.
- [71] B. Bunk, M. Della Morte, K. Jansen and F. Knechtli, Nucl. Phys. **B697**, 343 (2004), [hep-lat/0403022].
- [72] B. Bunk, M. Della Morte, K. Jansen and F. Knechtli, hep-lat/0408048.
- [73] A. Hart and E. Müller, Phys. Rev. **D70**, 057502 (2004), [hep-lat/0406030].
- [74] D. H. Adams, hep-lat/0411030.
- [75] D. H. Adams, Nucl. Phys. Proc. Suppl. **140**, 148 (2005), [hep-lat/0409013].
- [76] F. Maresca and M. Peardon, hep-lat/0411029.